Background Estimations in the Higgs to Four Leptons Decay Channel

A Study of Fake Lepton Efficiencies

Nuiok Dicaire

Supervisors:
Dr. Thomas Koffas
Dr. Ioannis Nomidis
Dr. William Leight

IPP Summer Student 2015 – Report

ABSTRACT

We present fake muon and electron efficiencies in the H->ZZ$^{(*)}$->4l channel calculated using the LHC data obtained during the month July 2015 corresponding to an integrated luminosity of 85 nb^{-1}. Given its low background and fully reconstructable final state, this channel is valuable for searches and measurements of the Higgs boson properties. Efficiencies are presented in control regions enhanced in light jets and conversion photons in the case of electrons, as well as in regions defined using cuts on the isolation and d0 significance variables in the case of both muons and electrons. These results will be used to extrapolate the light jets and photons contaminations in the signal region once more statistics are available.

I. TABLE OF CONTENTS

II. Introduction **3**

III. Background **3**

- **A) The Standard Model and the Higgs boson** 3
- **B) The LHC** 4
- **C) The ATLAS Detector** 4
- **D) Higgs production mechanisms:** 7
- **E) Production cross-section** 8
- **F) Higgs branching ratios** 9
- **G) The Higgs to four leptons channel** 9
- **H) Event Selection** 10
- **I) Background Estimations** 11
- **J) Fake lepton efficiencies** 12

IV. Results **13**

- **A) Important Variables** 13
- **B) The Method** 14
- **C) Control Regions** 14
- **D) Fake Electron Efficiencies** 15
- **E) Fake Muon Efficiencies** 17

V. Conclusion **18**

VI. References **18**

II. INTRODUCTION

One of the greatest accomplishment in physics in the past century is the development of the Standard Model (SM) of particle physics. This model incorporates the electromagnetic, weak and strong interactions and describes most of the known physics in terms of these interactions between the fundamental particles. However, some physical concepts and experimental observations, such as a unified theory of gravity, neutrino oscillations and dark matter are not explained in the context of the SM. Nonetheless, it is extremely accurate in predicting most of known physics.

With the discovery of the Higgs boson at the Large Hadron Collider (LHC), announced on July 4th 2012, one of the last missing pieces predicted by the SM was discovered. The goal is now to further study this new boson and its properties and ensure that it does correspond to the boson predicted by the SM. To determine the properties of particles at colliders such as the LHC it is crucial to know precisely how much background is measured.

Fake leptons efficiencies are crucial for background estimations. They are a measure of how often an event is wrongly determined to be signal due to an object being incorrectly identified as a lepton. In order to estimate this value in the signal region one uses control regions enhanced in specific background sources and composed of events distinct from those in the signal region.

In this work, we study the fake lepton efficiencies for muons and electrons in the Higgs to four leptons decay channel. An introduction to the essential physical concepts is presented in Section III. Results are discussed in Section IV, while conclusions are listed in Section V.

III. BACKGROUND

A) The Standard Model and the Higgs boson

The SM particles are six quarks and six leptons organized in three generations accordingly with their masses as shown in Figure 1. There are also four bosons that act as the carriers of the electromagnetic, strong and weak interactions. To this organized table of particles we need to add the Higgs boson, a scalar boson with an experimentally measured mass of 125 GeV, which is responsible for the mass of the fundamental particles through the Higgs mechanism.

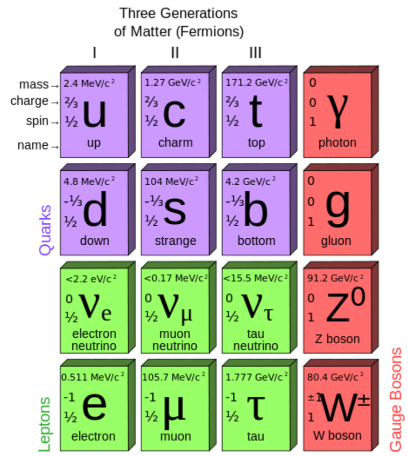

Figure 1[*]: The particles of the Standard Model; leptons, quarks and bosons.

B) The LHC

The Large Hadron Collider (LHC) is a proton-proton accelerator consisting of a 27 km ring of superconducting magnets with accelerating equipment and detectors, located approximately 100 m underground at the Swiss-French border. At four locations along its circumference, experiments detect and measure the properties of the particles created in up to 13 TeV (at the moment) centre-of-mass energy proton collisions. The four main experiments are ATLAS, CMS, LHCb and ALICE as seen in Figure 2. During the collisions, the energy that the proton carry can be used to produce new particles of larger masses than the initial hadrons through the known mass-energy equivalence. The result of the collisions is a shower of known SM particles in the detector but also of other types of exotic particles that could exist.

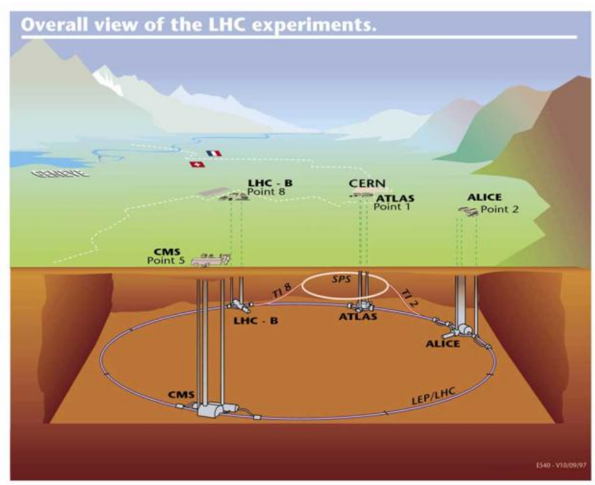

Figure 2[†]: The main experiments of the LHC.

C) The ATLAS Detector

The ATLAS detector, shown in Figure 3, must be able to determine the mass, momentum, charge, energy, spin, and lifetime of the particles. To accomplish this, the detector is made of different layers; the inner detector, the calorimeters and the muon spectrometer, each with specific tasks.

[*] www.realclearscience.com

[†] science.howstuffworks.com

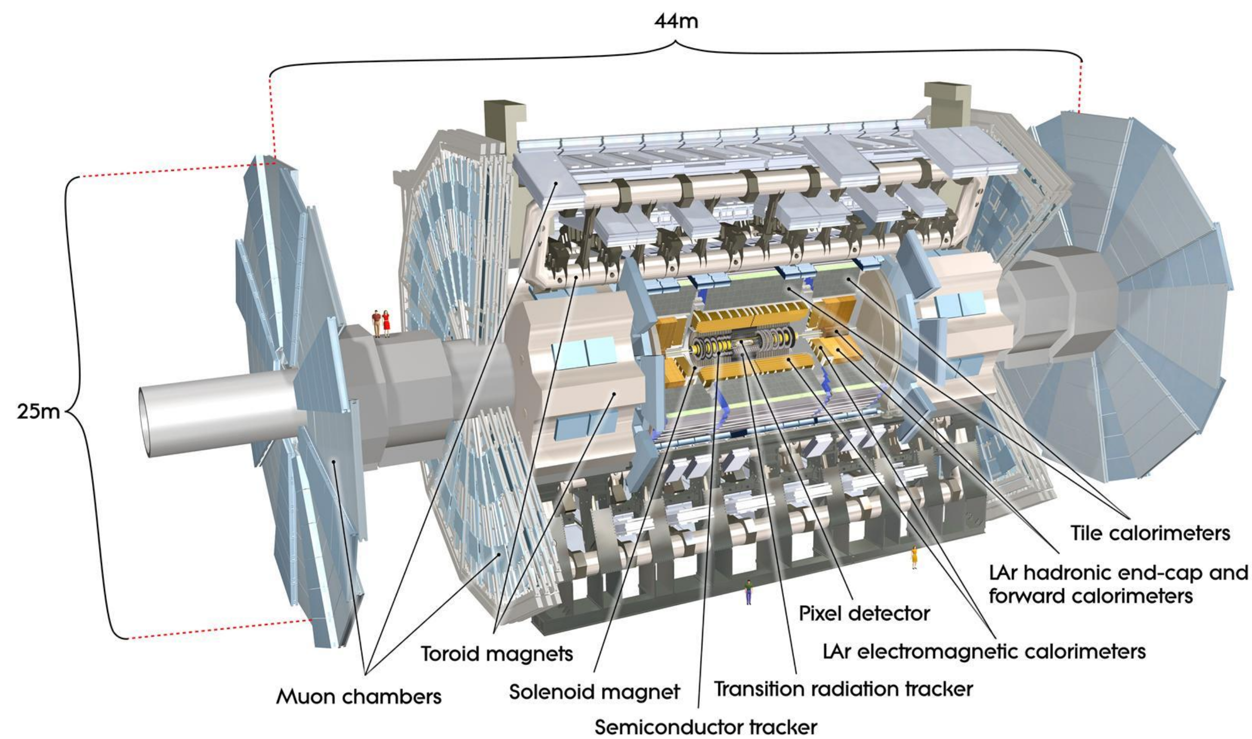

Figure 3: The ATLAS detector is composed of many different layers.*

i) ATLAS Coordinate System

The ATLAS experiment follows a right-handed coordinate system with the origin located at the nominal interaction point. The x-axis is defined as pointing toward the center of the LHC ring, the z-axis is horizontal along the beam and the y-axis points upwards.

The pseudo-rapidity, η, is the spatial coordinate that describes the angle of a particle relative to the beam axis. It is defined as

$$\eta \equiv -\ln\left[\tan\left(\frac{\theta}{2}\right)\right]$$

Where θ is the polar angle. Thus when θ is 90°, the pseudo-rapidity is also zero and goes to infinity as θ approaches zero. In the transverse plane the polar coordinates (r, ϕ) are used, where r is the distance to the beam pipe and ϕ is the azimuthal angle around the pipe.

ii) The Inner Detector

The inner detector tracks the charged particles and is the detector closest to the collision point. A central solenoid creates a 2 T magnetic field in that region that causes the charged particles to bend their trajectory. The direction gives the charge of the particle while the degree of curvature gives

* http://www.atlas.ch/photos/atlas_photos/selected-photos/lhc/9906026_01_layout_sch.jpg

information about the momentum. The inner detector can be subdivided into the pixel and semi-conductor silicon detectors and the transition radiation tracker. The silicon pixel detectors form the innermost part of the detector. They use silicon detectors in a similar fashion as to what is used in digital cameras to track the particles. When a highly energetic charged particle, for example an electron, passes through a silicon pixel it knocks out many electrons from the silicon without being stopped. The ejected electrons are then attracted in one direction by the electric field in the silicon pixel and hit the side of the detector, thus producing an electric signal. The small size of the pixels and their large number enables a precise tracking of the particles. Outside of the pixel detector is the semi-conductor tracker that operates in a very similar way to the pixel detector but is formed of long and narrow strips of silicon detector.

The outermost component of the inner detector is the transition radiation tracker. It is made of a large number of tubes, or straws, filled with gas. Between these straws is a material with a wide range of indices of refraction. When a relativistic charged particle passes through it emits transition radiations. The emitted photons then interact with the gas inside the tubes causing its molecules to emit electrons which are then pulled towards a central gold wire by an applied electric field where they leave a signal. Since different particles will produce different amount of radiation it is possible to distinguish between particles by measuring the strength of the signal. Lighter relativistic particles will tend to have a speed greater than the heavier ones and therefore will cause a higher amount of transition radiation. For example, an electron will produce a much stronger transition radiation than a pion.

iii) The Calorimeters

The calorimeters are placed outside the solenoid magnet that surrounds the inner detector. They measure the energy of the particles by absorbing it. There are two types of calorimeters. The innermost one is the electromagnetic (EM) calorimeter. It absorbs the energy of particles that interact through the EM interaction (i.e. electrons and photons). It consist of many layers of lead and stainless steel, the absorbers, with liquid argon cooled to 88 K in between them. When a high-energy electron passes through the calorimeter its very short wavelength enables it to interact with the quarks that compose the hadrons inside the absorbers. If a quark is ejected, because of color confinement as it is explained below, a shower of new particles, called a jet, will be created. A copper grid is placed in the argon and acts as an electrode to attract and measure the electrons produced when the shower of low energy particles ionizes the argon molecules. By measuring the energy of all the shower particles, it is possible to infer the energy of the initial particle. The calorimeter can also measure the angle between the beam axis and the particle's trajectory, as well as their trajectory within the perpendicular plane.

The next calorimeter is the hadronic calorimeter that measures the energy of particles that interact via the strong force. It is made of an array of steel and scintillator sheets, called tiles. The scintillators will emit light when exposed to charged particles. The high energy hadrons interact with the nuclei producing a shower of particles. These particles enter the scintillator and produce photons that are carried by optic fibers to devices where the light intensity is measured and converted into electric current. By measuring the intensity of the light, it is possible the determine the energy of the initial hadrons.

iv) The Muon Spectrometer

The last section of the ATLAS detector is a muon spectrometer. Since all other particles (except neutrinos) are stopped before they reach the muon spectrometer, all the signals detected are assumed to be muons. In order to obtain an accurate measurement the muon spectrometer has to be very large. It is made of gas tubes and operates in a similar fashion as the inner detector. As a muon passes through the detector it leaves a trail of positively charged ions and negatively charged electrons. By measuring the time it takes for the electrons to move from the ionizing point to the center of the tubes where they are detected, it is possible to determine the position of the muon as it passes through the detector. Toroidal magnetic fields are also used to bend the trajectory of the muons and measure their momentum.

D) Higgs production mechanisms:

In the Standard Model the Higgs boson is produced in the following modes in decreasing order of predicted production cross-section: gluon-gluon fusion (ggF), vector boson fusion (VBF), vector boson associated production (VH) and top quark associated production (ttH). Figure 4 presents the Feynman diagram of these processes.

a) <u>Gluon-gluon fusion (ggF):</u> Hadrons, such as protons which are accelerated in the LHC, are made up of quarks that are bound together by gluons. When the beams of accelerated protons collide, it is likely that two gluons will interact through a virtual loop that will produce a Higgs boson. This process has by far the most dominant contribution to the total Higgs production at the LHC.

b) <u>Vector boson fusion (VBF):</u> This process occurs when a quark-antiquark pair interacts through the exchange of a virtual W or Z boson which emits a Higgs boson. The characteristic signal of this process is a Higgs boson accompanied by two energetic jets in opposite directions.

c) <u>Vector boson associated production (VH):</u> The production of the Higgs boson from a quark-antiquark pair is accompanied by the production of a W or Z boson.

d) <u>Top quark associated production:</u> The production of the Higgs boson following the interaction of two gluons is accompanied by the production of a $t\bar{t}$ pair.

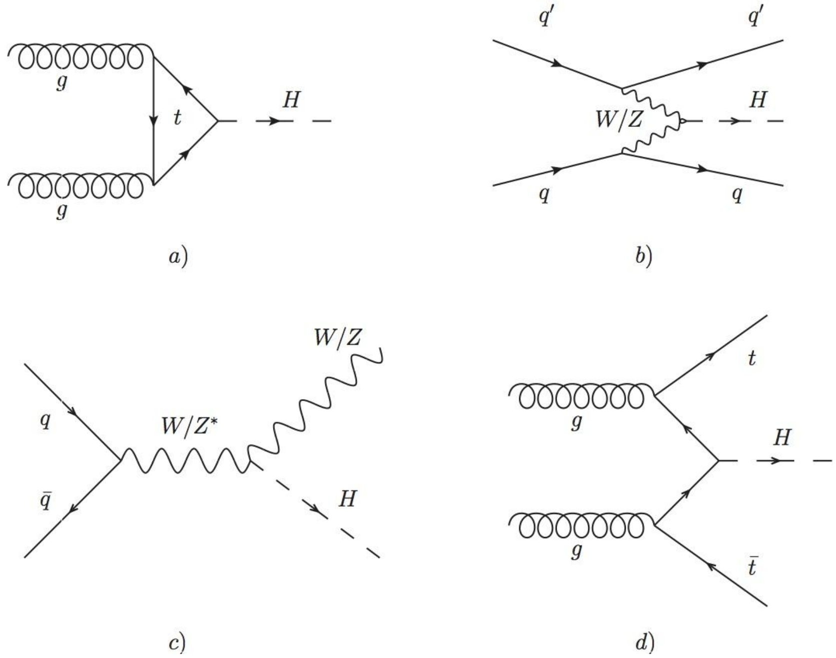

Figure 4[*]: Feynman diagram of a) gluon-gluon fusion (ggF), b) vector boson fusion (VBF), c) Vector boson associated production (VH), and d) Top quark associated production.

E) Production cross-section

Figure 5 presents the predicted cross-sections for the different production modes in pp collisions at a center of mass energy of 14 TeV. At 125 GeV, the main production mode is ggF, followed by VBF.

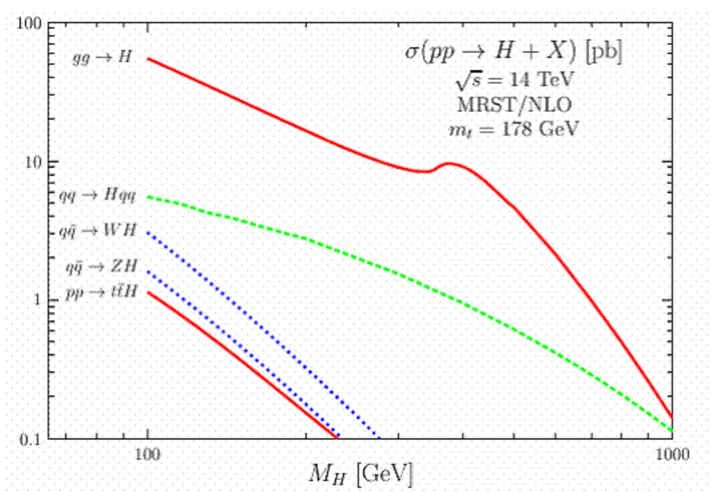

Figure 5[*]: The production modes of the Higgs boson and their respective probabilities as a function of the Higgs mass.

[*] www.beauty.ethz.ch/research/higgs

F) Higgs branching ratios

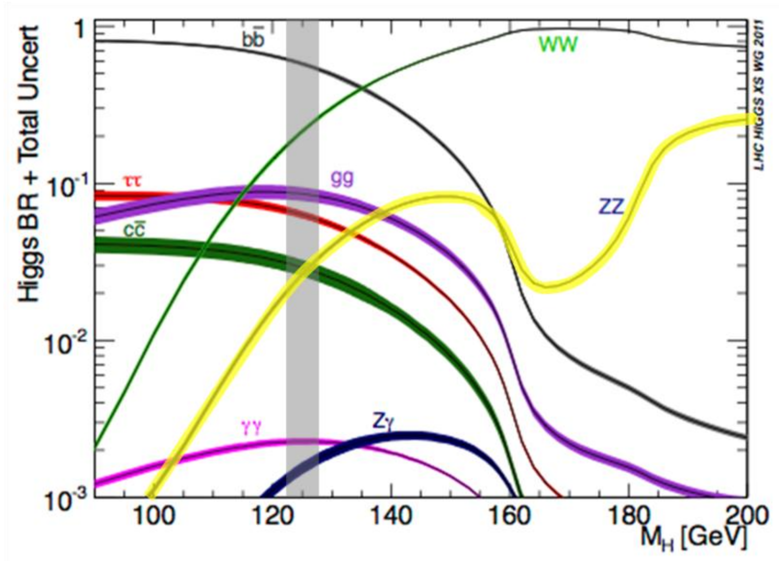

Figure 6[†]*: The Higgs decay channels and their branching ratios. The Higgs mass of 125 GeV is indicated in grey. The two Z boson decay mode used to obtain the 4 lepton final state is shown in yellow.*

The Higgs particle can decay through many different channels. The branching ratio for a given channel is defined as the fraction of the total number of decays that follow the process in question. It will depend on many different factors that are fixed by the SM, except for the mass of the Higgs boson. The dependence of the branching ratios for the different decays of the Higgs boson as a function of the mass of the Higgs is shown in Figure 6.

Below a mass of 130 GeV the Higgs dominantly decays to $b\bar{b}$ pair. At these low masses, where lies the Higgs mass of 125 GeV, many other decays modes have sufficiently high branching ratios to allow many different analyses and type of searches to look for the Higgs and study its properties.

G) The Higgs to four leptons channel

To detect new particles, one is searching for significant excesses above the predicted background. It is therefore essential to have an excellent understanding of the SM processes that produce similar or identical signals to the one for which one is looking.

As seen in Figure 6, the Higgs can decay to two Z bosons. The probability for a Z boson to decay to a lepton pair is about 3.4%. Thus the branching ratio for the 125 GeV Higgs boson to decay to a final state consisting of four leptons is 1.25×10^{-4}. Although this is much less likely to occur than a decay to $b\bar{b}$ or to two photons, this decay channel provides a clear signature in the detector with much less expected

[*] www.engineerdir.com/press/catalog/3824/

† atlas.ch

background. Moreover, the analysis is helped by the fact that no missing transverse energy is involved, thus making the reconstruction of a Higgs-like boson more precise.

The final state signature for this decay channel is the presence of four isolated leptons (two same flavor pairs with opposite charges) originating from the primary vertex. The first pair is selected such that is has a total mass closest to the Z mass of 91.187 GeV (i.e. on-shell Z boson). Figure 7 shows the mass distribution of the on-shell Z boson. Since the Higgs boson has been found at a mass of 125 GeV, the second Z boson must be off-shell.

Therefore, there are four distinct final states $\mu^+\mu^-\mu^+\mu^-$ (4μ), $\mu^+\mu^-e^+e^-$ (2μ2e), $e^+e^-\mu^+\mu^-$ (2e2μ), and $e^+e^-e^+e^-$ (4e). The difference between the 2μ2e and the 2e2μ final state is the flavor of the lepton pair that has a mass closest to that of the Z boson.

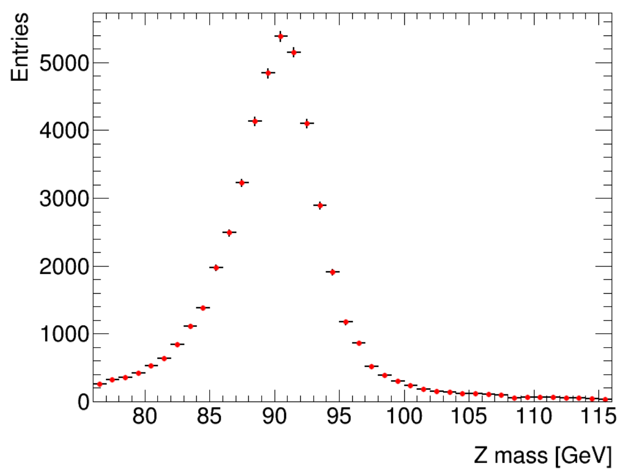

Figure 7: The mass distribution of the leading lepton pair.

H) Event Selection

To find leptons that might come from this 4l final state, the following selection criteria are applied. Muons are identified by matching the tracks in the muon spectrometer with the corresponding ones in the inner detector. On all the events that enter that category, a loose cut is applied, meaning that all the events that are more or less classified as muons are included, even if the probability of them actually being muons is somewhat low.

Additional cuts are also applied on the muons candidates. For example a transverse momentum (pT) of at least 6 GeV is required. The muons must be fairly close to the primary vertex in the transverse plane (a cut on the impact parameter significance, d0/σ(d0), is applied) and be sufficiently isolated. For a particle to be isolated, the total momentum (or energy deposited) of all the tracks within a cone of a given radius, *R*, around the particle in the inner detector (or the calorimeter) must be less than a predetermined cut that rejects a large fraction of leptons not coming from Z decays while retaining around 99% of leptons coming from the Z decay. The electron selection is similar, with a loose cut applied on the identification, a required minimal transverse momentum of 7 GeV, and isolation and impact parameter significance cuts.

I) Background Estimations

The background sources in the Higgs to four leptons channel can be divided into reducible and irreducible. The irreducible background consists of events that produce the same final state as the Higgs signal. For the H->4l channel, these are event where two Z bosons are produced by the annihilation of a quark-antiquark pair. The leptonic decay of these Z bosons will result in a four leptons final state, with the only difference from the Higgs signal being the intermediate Higgs boson, as seen in Figure 8. The contributions of this processe to the background can reliably be estimated using Monte Carlo (MC) simulations.

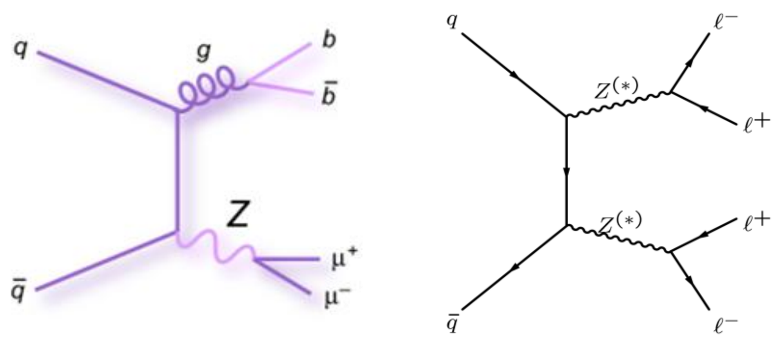

Figure 8[*]: Left: Example of a reducible background event where the jets formed by the b quarks would be misidentified as electrons. Right: Two Z bosons formed by two quarks decay into four leptons producing an irreducible background event.

The reducible background is dominated by Z+jets events. In these cases, a Z boson is produced in association with jets. If these jets are misidentified as leptons, this may lead to the same final four-leptons state as the signal. However, jets behave differently than leptons, thus have different properties which we exploit in order to reduce their contributions.

Other sources of reducible background include $t\bar{t}$ and WZ+jets events. Since reducible background are not physics-driven, the MC simulations do not provide accurate predictions them, thus data-driven methods using control regions are used in these cases.

Figure 9 shows the Higgs boson discovery plot from the ATLAS experiment in the Higgs to four leptons channel. This plot combines the data from the runs at 7 TeV and 8 TeV center of mass-energy. The backgrounds are shown in blue and purple, whilst the signal is shown in red.

[*] ATLAS public results

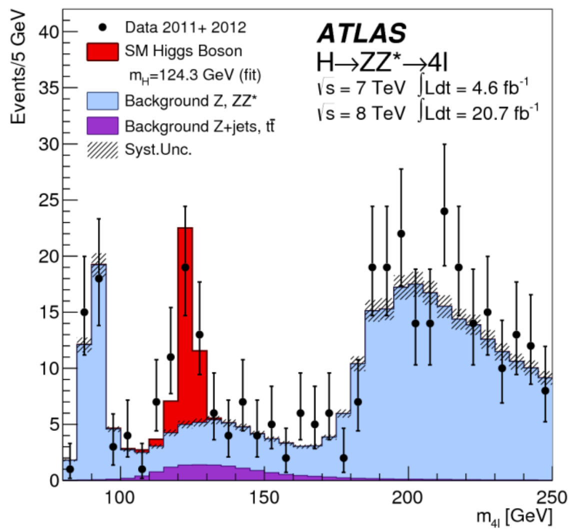

Figure 9[*]: Discovery plot of the Higgs boson in the four lepton channel. The reducible and irreducible backgrounds are shown is purple and blue respectively, while the excess above the predicted background (shown in red) is produced by the decay of the Higgs to four leptons.

J) Fake lepton efficiencies

In order to obtain good estimates of the background in the signal region, control regions orthogonal to the signal region (i.e. that do not contain any signal) and enhanced in a specific background are defined. The fake rate or efficiency in that control region, that is the ratio of events that are wrongly identified as electrons (or muons), is then used to extrapolated how many events are misidentified in the signal region.

These efficiencies are obtained as a function of pT and η. The equation below is used to calculate the fake rates in each of the pT and η bins. The total number of events that pass a given cut used to define the control region enhanced in a specific background is divided by the sum of the total number of events that pass and fail the same cut.

$$F = \frac{\#\,Pass}{\#\,Fail + \#\,Pass}$$

A larger fake factor therefore means that more fake events that are not electrons (or muons) pass the cut and are wrongly identified as electrons (or muons).

IV. RESULTS

A) Important Variables

The variable *nBL*, or the number of b-layer hits, is the number of hits recorded in the first layer of the Pixel detector. It is sensitive to photon conversions to electron-positron pairs that occur after the first layer of the Pixel detector. The total number of hits in the transition radiation tracker (TRT) is given by the variable *nTRT*, while the fraction of high threshold hits in the TRT is given by the variable *rTRT*. The electron high-threshold probability (*eProbHT*) is the probability of a high-threshold hit in the TRT. Figure 10 presents histograms of these quantities obtained using PowhegBox MC simulations. Different background sources are shown. Since these results come from MC simulations all background sources are known exactly.

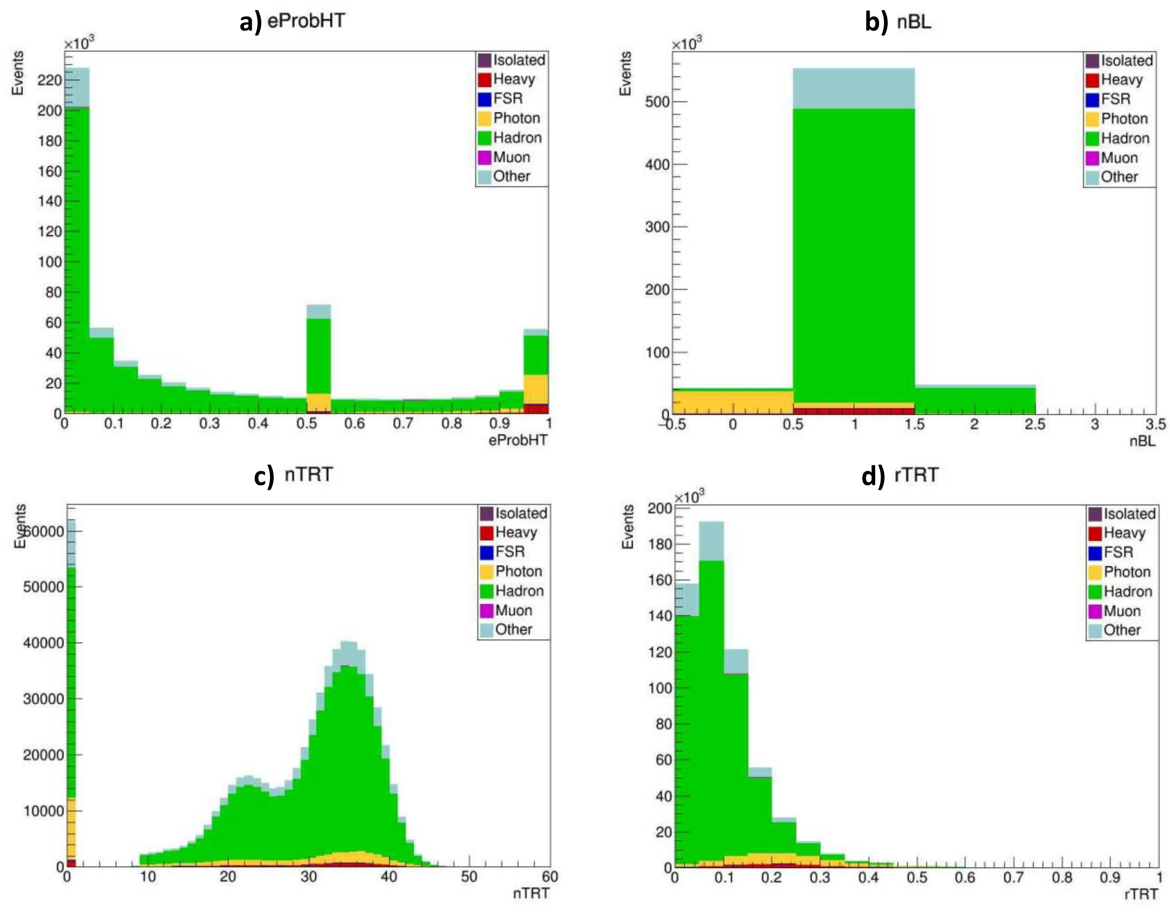

Figure 10: Variables describing quantities in the inner detector. a) The electron high-threshold probability, b) the number of b-layer hits, c) total number of hits in the transition radiation tracker, and d) fraction of high threshold hits in the TRT.

The number of hits in the b-layer (*nBL*) can be used to reject photon conversions, i.e. the e^+e^- pair production from a high energy photon. Indeed, these photons will produce zero hits in the Pixel detector and will then convert in the tracker, while electrons from the interaction point and hadrons will produce at least one b-layer hit.

Figure 10 shows the probability of high-threshold hits for electrons in the TRT. This probability depends on the Lorentz factor, $\left(1-\frac{v^2}{c^2}\right)^{-1/2}$. Relatively heavy pions and charged hadrons have a low probability of hits, around zero, while electrons have a probability much closer to one, which explains the distribution observed in the histogram of Figure 10. The excess of events observed at 0.5 is a default value for electrons and has no physical meaning. The distribution observed for the number of hits in the TRT (*nTRT*) is simply due to the characteristic shape of the transition radiation tracker.

B) The Method

A Z+X control region (CR) is defined with the usual selection criteria on the Z leptons and relaxed criteria on the additional X lepton. We then define CRs enhanced in each of the three main types of electron background we expect to see, namely photon conversions, misidentified light jets, and electrons from heavy flavor decays. To determine how much of each of these background types is present, we fit the distributions of the variables discussed above in data to distributions of those variables for each background type obtained from MC. Efficiencies obtained from the CR are then used to extrapolate these values to the signal region.

C) Control Regions

The Z+X control region is defined by selecting a dilepton pair using the normal selection criteria for a decaying Z boson. The X is an additional object that satisfies relaxed selection requirements. This so-called Z+X control region is used to estimate fake lepton efficiencies that are then used to extrapolate to the signal region using a 3l+X CR.

Conversion Enriched Z+X Control Region: A region enriched in photons is obtained by requiring zero hits in the b-layer (*nBL*=0). Figure 10 illustrates that the requirement *nBL*=0 provides a region with high purity in photons (93%). An additional cut on the ratio of the TRT hits over high threshold hits (*rTRT*) is applied in order to decrease the contamination in light jets. Indeed, Figure 10 shows that by requiring *rTRT*>0.1, a large fraction of light jets will be rejected.

Light Jets Enriched Z+X Control Region: To obtain a region enriched in light jets, a cut requiring at least one b-layer hit is applied. Once again, it is clear from Figure 10 that such a cut provides an excellent discrimination for light jets ("hadrons") and provides a CR with a purity of 97% in light jets.

Other Enriched Z+X Control Regions: Other regions enriched in other components, such as heavy flavored quarks, are difficult to obtain in the Z+X control regions thus, in this study, we limit ourselves to the ones described above.

D) Fake Electron Efficiencies

The fake lepton efficiencies were calculated separately for each of the background sources as a function of *pT* and *η*. Here we will look at the efficiencies for the light jets events and the photons events.

Fake lepton efficiencies were obtained for both the experimental data and MC simulations. The experimental data was taken at the LHC during the month of July 2015 at a center of mass energy of 13 TeV. Two types of Monte Carlo generators are used to simulate experimental data: PowhegBox and Sherpa. They are independent and provide different background estimation, it is thus useful to compare them both to the experimental data.

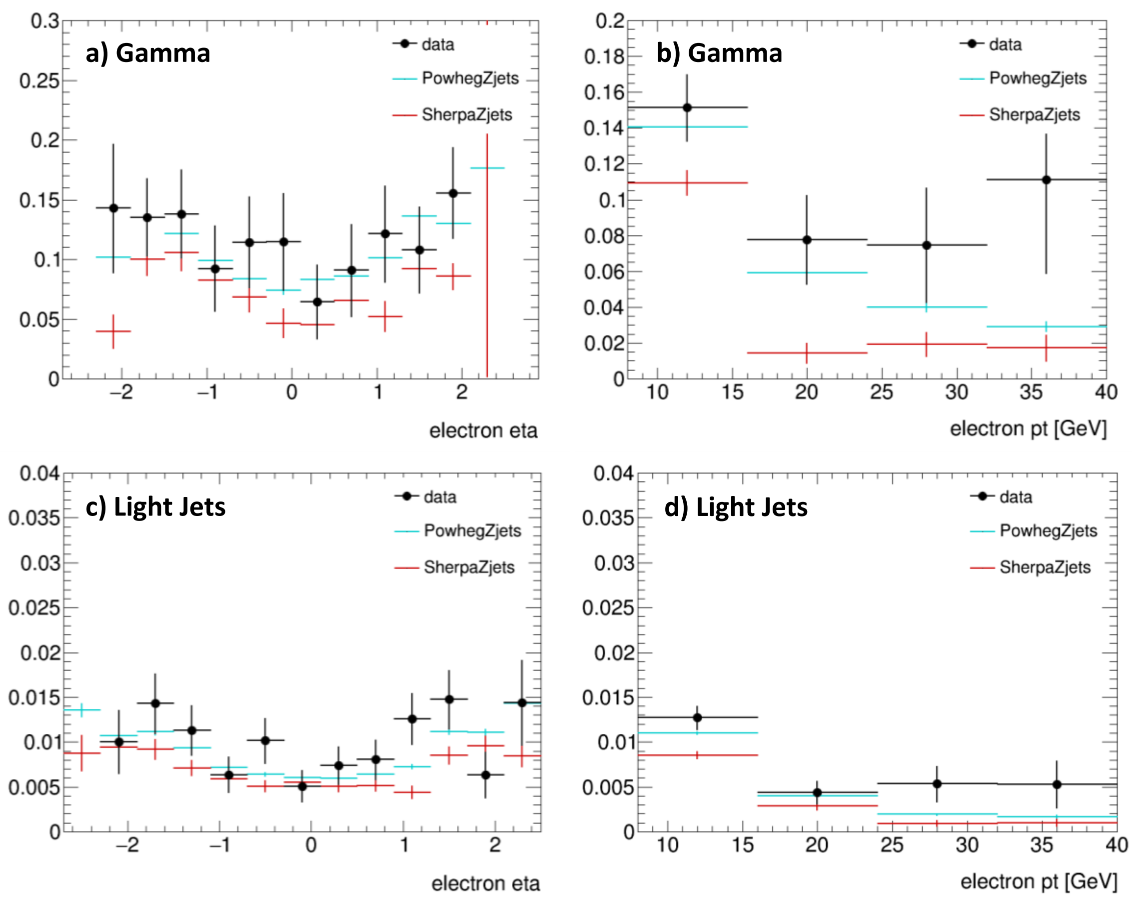

Figure 11: Fake electron efficiencies as a function of pT and η in CRs enhanced in light jets and photon conversion. The experimental data is shown is black. PowhegBox and Sherpa MC simulations are shown in blue and red respectively.

Fake electron efficiencies are calculated in the control regions enhanced in light jets and photons described above. In all cases, the Powheg MC simulations yield closer estimates to the experimental data although both Powheg and Sherpa somewhat underestimate the fake electron efficiencies. The efficiencies are shown as a function of *pT* and *η*.

When looking at the efficiencies as a function of the transverse momentum, we note that after a first drop, the efficiencies are more or less constant as the *pT* increases. The less energetic particles are indeed more likely to be misidentified as electrons. We also note that the fake rates for the photons are significantly larger than for the light jets.

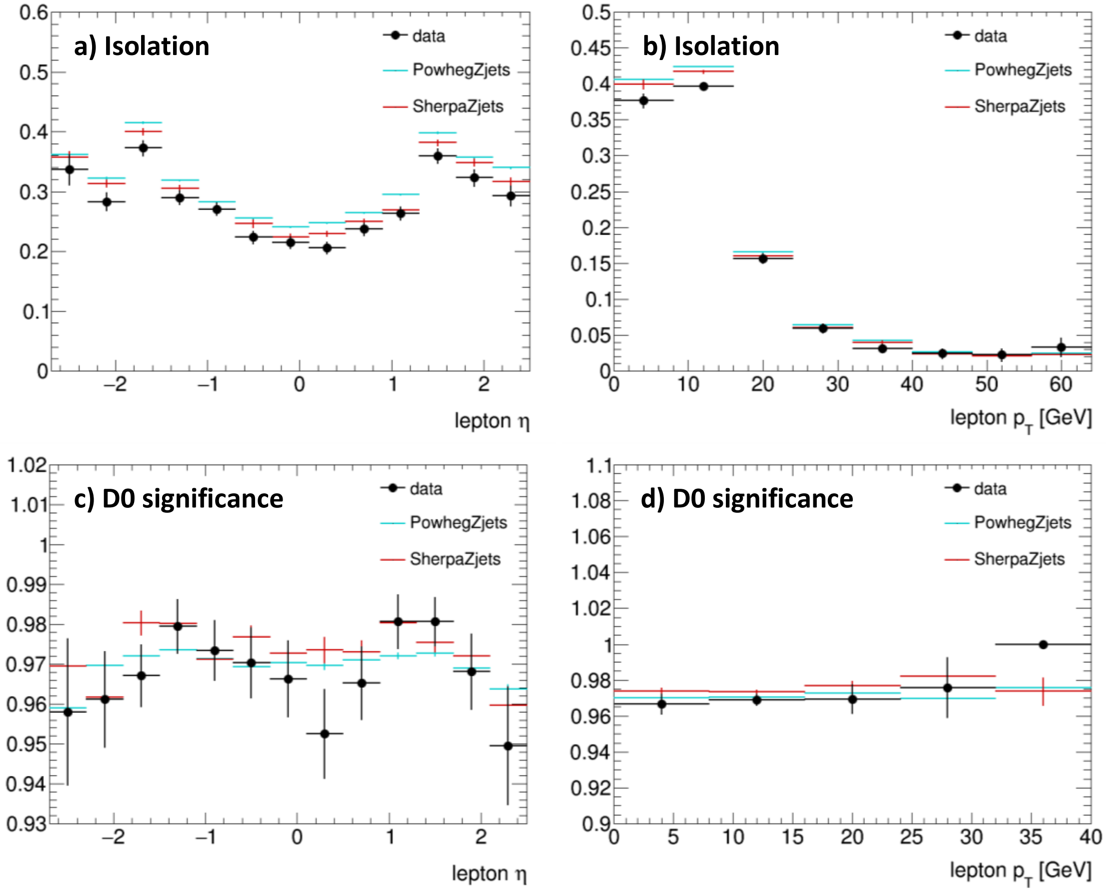

Figure 12: Fake electron efficiencies as a function of pT and η in CRs defined using cuts on the isolation and d0 significance. The experimental data is shown is black. PowhegBox and Sherpa MC simulations are shown in blue and red respectively.

Figure 12 a) and b) show the fake electron efficiencies obtained for events failing the isolation cut. All events passed both the impact parameter significance and the electron identification. Similarly, Figure 12 c) and d) show the efficiencies for the events that fail the d0 significance cut while passing both the isolation cut and the electron identification. The efficiencies are shown as a function of *pT* and *η*.

We first notice that all MC simulations tend to overestimate the efficiencies. The SHERPA MC simulations are somewhat closer to the experimental efficiencies in the isolation plots, while the POWHEG MC simulations yield slightly better estimates when using the d0 significance cut. The MC simulation do not correctly reproduce the efficiencies between values of 0 and 1 for η. We also note that the fake rates in the d0 plots are very close to 1 which implies that this cut barely rejects any events. In fact the very low statistics for these plots prevents us from drawing any meaningful conclusions from the plots shown in Figure 12 c) and d).

On the other hand, very good statistics are available for the plots showing the isolation efficiencies. The fake rate is especially high at low *pT* values but decreases quickly for more energetic events. This behavior is expected since highly energetic electrons have a more distinct signature in the detector and are less likely to be produced by non-interesting interactions. The characteristic shape observed for the *η* efficiencies reflects to the amount of material traversed in the detector. Nonetheless, the fake rates in both isolation plots reach values up to 0.4 which means that a significant number of events are misidentified as electrons in these control regions.

E) Fake Muon Efficiencies

Figure 13 shows the muon efficiencies obtained for events failing the isolation cut or the impact parameter significance. The statistics are significantly lower than for electrons and as such, no significant conclusion can be extrapolated from the fake rates.

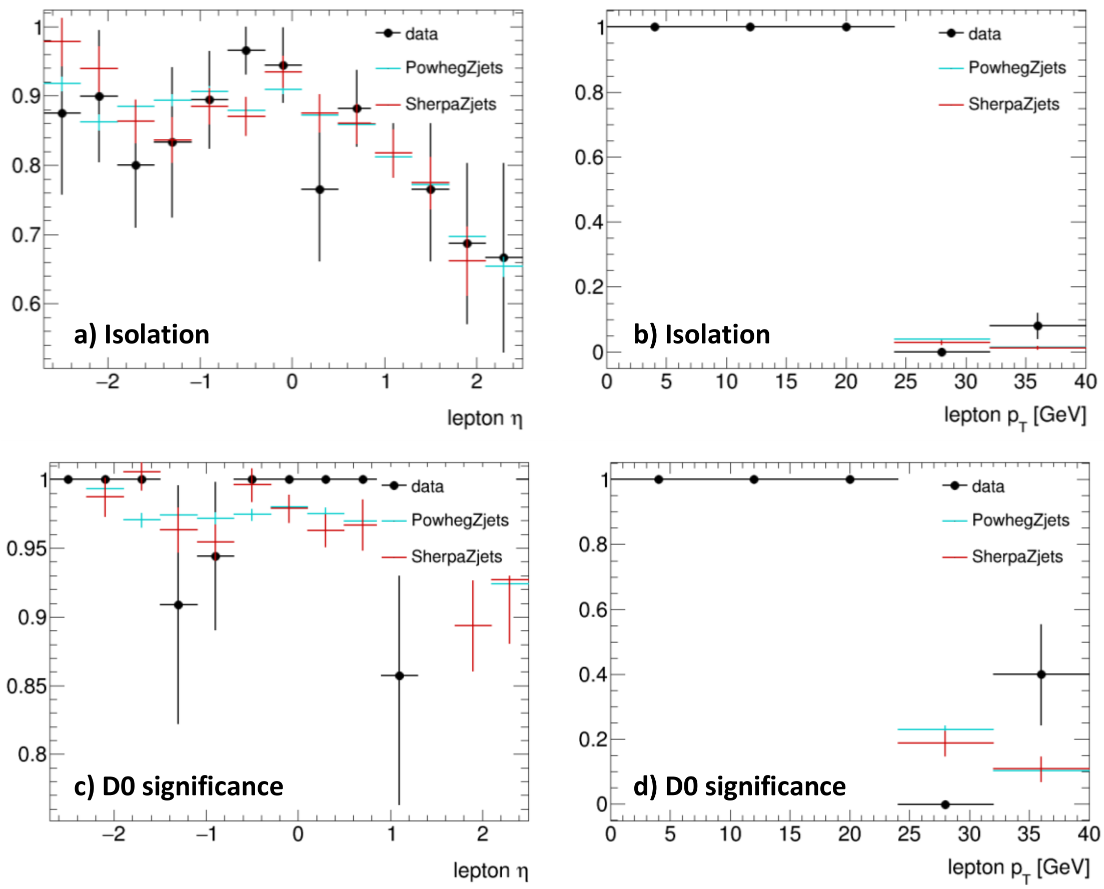

Figure 13: Fake muon efficiencies as a function of pT and η in CRs defined using cuts on the isolation and d0 significance. The experimental data is shown is black. PowhegBox and Sherpa MC simulations are shown in blue and red respectively.

V. CONCLUSION

We performed a complete study of fake electron and muon efficiencies using the data collected at the LHC during the month of July 2015 at 13 TeV, with a total integrated luminosity of 85 nb^{-1}. The efficiencies were calculated using the MC PowhegBox and Sherpa data. The MC simulations tend to systematically over or underestimate the efficiencies.

For the electrons we used two control regions enhanced in conversion photons and light jets respectively. In addition the efficiencies were calculated in two regions defined by using a cut on the isolation and the d0 significance respectively. The patterns observed when looking at the electron efficiencies as a function of pT and η are consistent with what one would expect, while the results for muons were somewhat harder to interpret given the lack of available statistics.

Future work will focus on implementing a CR enhance in heavy flavored jets using b-jet tagging algorithms in order to also obtain the efficiencies for this background. These results will then be use to extrapolate the fake rates in the signal region. The variables such as the ones presented in Section IV A) will be fitted to data in order to obtain the fractions of each type of background in the data. This will be used along with the efficiencies to determine the number of misidentified leptons in the signal regions. Developing such an understanding of the behavior of the background is essential to detect new particles and study their properties. This work will be completed when more data from the LHC will provide more statistics.

VI. REFERENCES

ATLAS Collaboration, *ATLAS Detector and Physics Performance*. ATLAS TDR 14, CERN/LHCC 99-14, Issue 1, 1999.

ATLAS Collaboration, *ATLAS Experiment at the CERN Large Hadron Collider.* IOP Publishing and SISSA 2008.

ATLAS Collaboration, *Measurement of the Higgs boson mass from the H->γγ and H->ZZ^*->4l channels with the ATLAS detector using 25 fb-1 of pp collision data*. Phys. Rev. D 90, 052004 (2014).

ATLAS Experiment – Public Results [Online] twiki.cern.ch/twiki/bin/view/AtlasPublic/WebHome, (consulted on 9/10/15).

CERN, *Physics*. [Online] home.web.cern.ch/about/physics, (consulted on 9/10/15).

CERN, *The Larger Hadron Collider*. [Online] home.web.cern.ch/topics/large-hadron-collider, (consulted on 9/10/15).

Lacuesta, V. *Track and vertex reconstruction in the ATLAS experiment*. JINST (2013) 8 C02035.

Strassler, Matt. *Of Particular Significance: Conversations About Science with Theoretical Physicist Matt Strassler*. [Online] profmattstrassler.com, (consulted on 9/10/15).